Effects of transverse jet parameters on flame propagation and detonation transition in hydrogen–oxygen-argon mixture

Han Peng[a, b], Yue Huang [a*], Ralf Deiterding[b], Yancheng You[a], and Zhenye Luan[a]

[a] *School of Aerospace Engineering, Xiamen University, Xiamen, China;* [b] *School of Engineering, University of Southampton, Southampton, United Kingdom*

∗Corresponding author: Ph.D., Associate Professor, Tel.: 86-592-2182460; Fax: 86-592-2182460

E-mail address: huangyue@xmu.edu.cn.

Effects of transverse jet parameters on flame propagation and detonation transition in hydrogen–oxygen-argon mixture

Two-dimensional numerical simulation is performed with the open-source program AMROC to study the effects of transverse jets (act as fluidic obstacles within a detonation tube) on the flame acceleration and deflagration to detonation transition (DDT). The slot transverse jets have been studied and compared with conventional solid obstacles in tubes. The jet initial parameters, such as mixture composition, stagnation temperature, pressure and mass flow rate, are investigated. The results demonstrate that a hydrogen-oxygen-argon reactive fluidic obstacle leads to the shortest DDT distance and time compared with solid obstacles and fluidic obstacles composed of pure oxygen or argon. The fluidic obstacles can induce more vorticities to accelerate flame propagation. The DDT distance and time decrease with the jet initial temperature, pressure and mass flow rate rise, while a high jet initial stagnation temperature is counterproductive to shorting DDT distance and time. The local static pressure rise plays an important role in flame acceleration when increasing the initial pressure of the fluidic obstacle. Higher jet pressure and a wider jet induce more compression waves, which can make the initial flame front more unstable and accelerate the flame as well.

Keywords: flame acceleration; DDT; transverse jets; fluidic obstacles; flame-vortex interaction;

Introduction

As a new energy source with broad prospects in the future, hydrogen has the advantages of no emission during the production process, excess reserves, higher calorific value and zero potential emission in combustion process (Eichert and Fischer, 1986). A large number of experimental, theoretical and numerical studies have been undertaken in order to understand the nature of the hydrogen deflagration to detonation transition. These studies are inspired by their importance for industrial safety including prevention of explosion during the hydrogen production and storage process and their potential application for propulsion and power devices (Roy et al., 2004; Petukhov et al., 2009).

In the propulsion area, solid obstacles, like orifice plates and Shchelkin spirals, have been used in pulse detonation engines (PDE) and pre-detonation tubes of rotating detonation engines (RDE) to effectively accelerate the flame propagation and shorten the run-up distance and time to detonation (Lee, 2008; Lee et al., 2004). Research shows that a solid obstacle in a detonation duct can form a reverse flow zone behind it and enhance the turbulent intensity downstream (Ciccarelli and Dorofeev, 2008; Oran and Gamezo 2007; Gamezo et al., 2007; Ayu et al., 2018). However, there are some disadvantages in using solid obstacles. For instance, the pressure losses caused by those solid obstacles have negative influences on thrust performance of multicycles PDE and the obstacles also act as thermal reservoirs, exchanging heat at improper time in the detonation tube and make the operation unstable. Therefore, the design of obstacles in detonation engine for shorting DDT distance and time needs to balance the flame acceleration gain and the total pressure loss (Kessler et al., 2010; Gamezo et al., 2008; Johansen and Ciccarelli, 2010). The transverse jet is proposed as a new kind of obstacle, namely the fluidic obstacle, to initiate a detonation wave due to its relatively low total pressure loss (Knox, 2011).

The transverse jet or fluidic obstacle induces a series of coherent vortices and mass entrainment (Yuan and Street, 1998; Karagozian and Ann, 2014), which interact with the flame upstream resulting in local flame acceleration and detonation transition. Several relevant experiments were carried out to study the effect of fluidic obstacles on the DDT process (Knox et al., 2010; Knox et al., 2011). When the main flow consisted of a stoichiometric hydrogen-air mixture and the fluidic obstacle composition was either premixed stoichiometric hydrogen-air or pure air, the results showed that the jet plays the role of a virtual obstacle but induces substantially lower total pressure losses than a solid obstacle with similar blockage shape. Experiments about the fluidic obstacle made by pure air and kerosene-air were carried out to investigate the effect of jet on local fuel-air

ratio, which indicated that a pure air jet deteriorates the local kerosene-air ratio and has an adverse influence on flame propagation. On the other hand, a jet made by a kerosene-air mixture can effectively accelerate the flame propagation (Zhao et al., 2017). The methane-air flame acceleration and DDT process in a duct with jet in crossflow was experimentally studied by PIV and Schlieren photography, which showed that the fluidic obstacles are more effective at transitioning the laminar flame to a turbulent flame than the solid obstacles. The research about the fluidic obstacle influence on the primary stages of the DDT process indicated that the fluidic obstacle increases turbulent intensity through the interaction between the jet and the flame. The jet entrainment mechanisms and the flow instabilities were strengthened with the jet flow, leading to higher flame velocity (McGarry and Ahmed, 2015; Chambers and Ahmed, 2017; McGarry and Ahmed, 2017). Apart from that, a special jet cavity was designed and numerically studied to form a high-pressure zone in the detonation tube and ignite the detonation through multiple shock reflections on the wall (Wang, et al., 2017). Our own former research focused on the reactive fluidic obstacle location, duration and arrangements, where these factors were found to be important for the DDT process and were investigated by experiments and numerical simulations (Peng et al., 2018). However, the effects of the transverse jet parameters on the DDT processes, such as jet mixture composition, temperature, pressure, width and flow characteristics, need to be further investigated by experiments and numerical simulations.

Because DDT needs a long distance, while the flame develops and propagates very quickly, existing experimental methods are not sufficient to capture the entire flow field with high resolution. High-resolution numerical simulation on the other hand is a feasible and safe way to get details about the flow field and flame evolution in the DDT process. Two- and three-dimensional simulations with a one-step Arrhenius chemical

model or a detailed chemical mechanism both showed that solid obstacles in a detonation tube can induce vorticities and thus enhance the turbulent intensity downstream (Gamezo et al., 2008; Johansen and Ciccarelli, 2010; Ayu et al., 2018). However, using the one-step chemistry model in detonation simulations introduces uncertainties on some properties of the flame, such as the induction time in chain-branching kinetics, detonation initiation and the overdriven surface instability (Zeldovich, 1980; Liberman et al., 2010; Zhang et al., 2018). The initial thermal diffusion and hydrodynamic instability play significant roles in flame acceleration. In comparison, solid obstacles reflect the precursor shock resulting in hot spots in the preheat region. The hot spots and the local concentration gradient are considered as the main mechanism to trigger the transition to detonation. The SWACER (the shock wave amplification by coherent energy release) mechanism and the Zeldovich gradient mechanism suggest that a suitable temperature gradient can be formed between the flame front and the precursor shock wave and trigger the detonation (Lee and Moen, 1980). Shock wave-boundary layer interactions are also found being key for auto-ignition in the boundary layer in a smooth tube (Edyta and Hayashi, 2013). However, the influence of the initial parameters of the fluidic obstacle on the flame propagation in a DDT process with detailed chemistry model has not yet been explored by numerical simulations.

There are few publications about the effects of the initial parameters of fluidic obstacles on the DDT process by either experiments or numerical simulations. In this paper, two-dimensional direct numerical simulations with a multi-step hydrogen-oxygen-argon chemical kinetics mechanism are carried out to study the flame acceleration process in a detonation duct with a reactive transverse slot jet in crossflow as fluidic obstacle. The comparison between fluidic obstacle and solid obstacle is firstly studied. Then the jet

injection parameters are fundamentally investigated, including jet mixture composition, temperature, pressure and width.

Numerical specifications

Numerical methods

The two-dimensional viscid unsteady reactive Navier-Stokes equations with perfect gas equation of state are solved as the governing equations，

$$\frac{\partial Q}{\partial t}+\frac{\partial\left(F_x-G_x\right)}{\partial x}+\frac{\partial\left(F_y-G_y\right)}{\partial y}=S \tag{1}$$

here Q is the state quantity, F_x and F_y are the convection fluxes, and S is the source term of chemical reaction, which is defined as follows:

$$Q=\begin{bmatrix}\rho_i\\ \rho u\\ \rho v\\ \rho E\end{bmatrix},\quad F_x=\begin{bmatrix}\rho_i u\\ \rho u^2+p\\ \rho uv\\ u\left(\rho E+p\right)\end{bmatrix},\quad F_y=\begin{bmatrix}\rho_i v\\ \rho uv\\ \rho v^2+p\\ v\left(\rho E+p\right)\end{bmatrix},\quad S=\begin{bmatrix}\dot{\omega}_i\\ 0\\ 0\\ 0\end{bmatrix}, \tag{2}$$

where i = 1, 2, ..., n. n is the total species number, ρ_i is the density of component i. In equation (1), G_x and G_y are diffusion fluxes, which are defined as follows:

$$G_x=\begin{bmatrix}\rho D_i\dfrac{\partial Y_i}{\partial x}\\ \tau_{xx}\\ \tau_{xy}\\ k\dfrac{\partial T}{\partial x}+\rho\sum_{j=1}^{N_{sp}}h_j D_j\dfrac{\partial Y_j}{\partial x}+u\tau_{xx}+v\tau_{xy}\end{bmatrix} \tag{3}$$

$$G_y = \begin{bmatrix} \rho D_i \dfrac{\partial Y_i}{\partial y} \\ \tau_{yx} \\ \tau_{yy} \\ k\dfrac{\partial T}{\partial y} + \rho\sum_{j=1}^{N_{sp}} h_j D_j \dfrac{\partial Y_j}{\partial y} + u\tau_{xy} + v\tau_{yy} \end{bmatrix} \tag{4}$$

In the latter, Y is the mass fraction, $k\dfrac{\partial T}{\partial x}$ 、 $k\dfrac{\partial T}{\partial y}$ are convention flux terms，

$\rho\sum_{j=1}^{N_{sp}} h_j D_j \dfrac{\partial Y_j}{\partial x}$ 、 $\rho\sum_{j=1}^{N_{sp}} h_j D_j \dfrac{\partial Y_j}{\partial y}$ are diffusion flux terms, τ is the viscosity stress and the stresses in all direction are

$$\tau_{xx} = -\frac{2}{3}\mu\left(\nabla\cdot\mathbf{v}\right) + 2\mu\frac{\partial u}{\partial x}, \quad \tau_{yy} = -\frac{2}{3}\mu\left(\nabla\cdot\mathbf{v}\right) + 2\mu\frac{\partial v}{\partial y} \tag{5}$$

$$\tau_{xy} = \tau_{xy} = \mu\left(\frac{\partial u}{\partial y} + \frac{\partial v}{\partial x}\right), \quad \nabla\cdot\mathbf{v} = \left(\frac{\partial u}{\partial x} + \frac{\partial v}{\partial y}\right). \tag{6}$$

Besides，E in equation (1) indicates the total unit energy,

$$E = \sum_{i=1}^{N_{sp}} Y_i h_i - \frac{p}{\rho} + \frac{1}{2}(u^2 + v^2), \tag{7}$$

where h_i is the specific enthalpy of species i, which reads

$$h_i = h_{ref}^0 + \int_{T_{ref}}^{T} C_{p_i} dT. \tag{8}$$

$\dot{\omega}_i$ is the mass generation rate of component i, which can be calculated by a chemical reaction mechanism of J steps as

$$\dot{\omega}_i = \sum_{j=1}^{J} \left(\nu_{ji}^{r} - \nu_{ji}^{f} \right) \left[k_j^f \prod_{n=1}^{N_{sp}} \left(\frac{\rho_n}{W_n} \right)^{\nu_{jn}^f} - k_j^r \prod_{n=1}^{N_{sp}} \left(\frac{\rho_n}{W_n} \right)^{\nu_{jn}^r} \right], \; i = 1, \ldots N_{sp}. \qquad (9)$$

The rate constant of forward and reverse chemical reaction is given by the Arrhenius formula:

$$k_j^{f/r}(T) = A_j^{f/r} T^{\beta_j^{f/r}} \exp\left(-\frac{E_j^{f/r}}{RT} \right) \qquad (10)$$

In equation (10), the activation energy and pre-exponential factor come from the corresponding chemical reaction mechanism. The ideal gas equation is used to close the overall system, i.e. equation (1).

The open-source program (Deiterding, 2003) AMROC (Adaptive Mesh Refinement Object-oriented C++) was adopted for the simulations. The reactive flow solver within AMROC has been validated for parallel numerical simulations of multi-dimensional detonation combustion in several studies (Deiterding, 2009; Ziegler et al., 2011; Deiterding and Wood 2013; Cai et al., 2016; Cai et al., 2018; Wang et al., 2018).

A hybrid Roe-HLL Riemann solver is utilized to construct inter-cell numerical upwind fluxes. The Minmod limiter with MUSCL reconstruction is applied to construct a second-order method in space. A conservative second-order accurate centered difference scheme is used for the diffusive term. A first-order accurate Godunov splitting method is adopted for the source term and a semi-implicit generalized Runge–Kutta method of fourth order (GRK4A) is utilized for the integration of the chemical kinetics (Deiterding, 2003). A detailed chemical kinetic mechanism (Westbrook, 1982) for H2/O2/Ar was used to model the chemical reaction of the DDT process. The mechanism contains 9 species and 34 elementary reactions, and it has been used to simulate detonation combustion successfully.

Simulations setup

The computational domain is a two-dimensional rectangular channel with a length of 800 mm and a width of 20 mm. As Fig. 1 shows, the tube is closed at the left end (x = 0) and open to the atmosphere at the opposite end (x = L). The top and left walls are adiabatic no-slip walls, while the right boundary is set as outflow boundary condition. The jet injection position and solid obstacle are located at the bottom wall and 50 mm from the left end. A planar laminar flame, its detailed structure calculated by CHEMKIN in advance, is initialized to ignite the unburned mixture weakly. The unburned mixture's temperature is set to 300 K and the pressure in the whole fluid domain is set to 0.1 MPa. The initial stoichiometric hydrogen-oxygen mixture in the simulations is diluted with 50% argon. Note that the cases with different injection composition, temperature, pressure and width are introduced in section 3. Pressure ratio (PR) is defined as the ratio of the initial stagnation pressure of a fluidic obstacle to the initial pressure of the stationary flow field. A typical solid obstacle with blockage ratio (BR) of 0.5 is shown in Fig. 1. All temperature values T_{jet} in this paper refer to the stagnation temperature and P_{jet} always refers to the stagnation pressure.

Verification of mesh resolution and convergence

The computational base cell size is set to 0.5 mm × 0.5 mm and refined with 5 levels (refinement factors are 2, 2, 2, 2) to 0.03125 mm × 0.03125 mm adaptively on-the-fly. The case with a single reactive fluidic obstacle is used to verify the numerical results with differently refined meshes. The laminar flame thickness is about 0.515 mm for the current initial conditions, as calculated by Cantera (Goodwin, 2019). The minimum mesh size is 0.03125mm, about 16 grid points per laminar flame thickness (16 pts/L_l). A resolution study was conducted with three differently refined meshes corresponding to 8 to 32 grid points per laminar flame thickness. As Fig. 2 shows, the local detonation in the coarse

mesh case (Level 4) occurs earlier than in the more refined cases (Level 5 and 6). The details of the flow field, like the flame front and pressure waves, can be dynamically captured only by the finer meshes.

The criterion for a detonation should be the presence of shock wave closely ahead and directly coupled to the flame. A detonation is defined as a self-sustained shock-induced combustion front (versus thermally induced combustion). In this paper, if the flame propagation speed is greater than or equal to the C-J velocity, the flame is considered to be transformed into an overdriven or a C-J detonation, respectively. The distance between the left wall and the location of primary local detonation is defined as the DDT distance. The time when the primary local detonation was ignited is defined as the DDT time.

Figure 3 shows the flame front velocity. The location where DDT occurs is closer to the left boundary when the mesh is relatively coarse (8 pts/L_l). The flame front, DDT distance and time become more reliable when the minimum mesh size is decreased. Although there are still some differences between the results of the cases with 16 pts/L_l and 32 pts/L_l, these computations differ by less than 1% and 6% in DDT time and distance, respectively. This shows that the calculations of the two-dimensional flame acceleration and DDT process are gradually converging.

It is found that a minimum spatial resolution of 3 to 4 cells number per laminar flame thickness length is necessary to accurately resolve the DDT process. For multi-dimensional calculations, the resolution from 5 to 10 cells per laminar flame thickness has practically no effects on the flame acceleration (Gamezo et al., 2007; Gamezo et al., 2008; Kessler et al., 2010). But a recent high-resolution numerical simulation shows that the calculation result depends on the spatial resolution until there are more than 30 cells per laminar flame thickness (Han et al., 2017). However, it is noted that in larger channels

and engineering applications, the minimum cell size is limited by the available computational resources. In this paper, the five-level refinement (16 pts/L_l) is used in all the calculations, which balances the simulation resolution and computing effectiveness. All calculations were performed on a high performance computing cluster in the School of Aerospace Engineering in Xiamen University, where 28 cores (Xeon E5-2680v4 2.4GHz) were used for each case. Typical runtimes for a whole DDT process were proximately 6 to 7 days wall-clock time.

Results and discussions

Comparison of flame propagations within smooth, solid obstacle and fluidic obstacle tube

Figure 4 shows the velocity distribution along the length of smooth pipe with no obstacles, single solid obstacle (BR = 0.1, BR = 0.5) and single fluidic obstacle (T_{jet} = 300K, P_{jet} = 0.3MPa, PR = 3), respectively. The propagation process of a premixed flame in the tube is divided into four stages. The first stage is the laminar flame acceleration process. After gentle ignition, the flame propagates in the form of a laminar flame, and the flame propagation speed is slow at this stage. The second stage is that the flame surface is deformed and folded, which is affected by the boundary layer and the expansion of combustion products. At the third stage, due to the increase of reaction rate and energy release in the front of the flame, a strong shockwave is formed downstream. The region between flame front and the shockwave is preheated and local detonation occurs in the turbulent flame, preheated region or boundary layer, which is called the explosion center or hot spot. In the last stage, local hot spots transform into a global detonation. The flame accelerates rapidly, resulting in overdriven detonation, and then the detonation wave speed decreases with a fluctuation near the CJ theoretical velocity.

As shown in Fig. 4, the distance required for flame transition to detonation is shortened after adding obstacles, and the effect of fluidic obstacles on flame acceleration is more obvious than that of solid obstacles, which is consistent with the former experimental and numerical results (Gamezo et al., 2008; Knox et al., 2010; Knox et al., 2011). The dotted line in the figure shows the position of the obstacle. At the first stage, the flame propagates at the same velocity in the three cases. The flame accelerates in the tube with fluidic or solid obstacle when passing through the obstacle. Due to the high blocking ratio (BR = 0.5), the flow area of the pipe suddenly decreases by half, so the flame propagation speed needs to rise. Then the flame expands into the radial direction and the flame propagation speed shows a drop accordingly. When the blocking ratio is relatively low (BR = 0.1), the effect of the solid obstacle on flame acceleration is limited.

Figure 5 shows the streamline distribution of the flow field when the flame passes over the obstacle. As the left picture shows, expansion of the burned gas leads to the movement of unburned gas and forms vortices downstream of the obstacle. The vortices gradually develop into a large recirculation zone. When the flame passes over the solid obstacle, it is entrained in the recirculation zone, and the flame is accelerated temporarily by the shear stress of the vortices. The extend of the recirculation zone is larger when the blocking ratio is higher. In this paper, the effective blocking ratios of solid obstacle (BR = 0.1) and fluidic obstacle (PR = 3) are similar. Compared with solid obstacles, the fluidic obstacle induces a series of vortices by itself after being injected into the tube. The interaction with unburned gas will move downstream continuously and flame-vortex interaction is an important factor for fluidic obstacles to accelerate the flame (McGarry and Ahmed, 2015).

Multiple obstacles are more likely used in DDT experiments because the effect of a single obstacle is limited. Figure 6 (a) shows the density gradient contour of the flow

field as the flame passes through six obstacles. In the process of flame propagation to the right, movement of the unburned gas is promoted. Due to the existence of solid obstacles (BR = 0.5), a series of smaller vortices is induced downstream, and recirculation zones are formed in the cavities between the obstacles.

As shown in Figure 6 (b), a series of complex vortices is formed after the six impinging fluidic obstacles (T_{jet} = 300K, PR = 3) are injected into the flow field. The first leading mushroom vortices move upstream and interact with the flame surface. Influenced by the vortices formed by the fluidic obstacles, the flame surface develops into a funnel-like shape, and a large unburned pocket is formed in the burned region. The flame surface is wrinkled and distorted by Rayleigh-Taylor instabilities and its total area is increasing. Also the overall heat release rate increases, which leads to further acceleration of the flame.

Figure 7 shows the pressure profile of the flow field with multiple obstacles at the time when the local explosion is triggered. For a tube with multiple solid obstacles, local explosions occur on the flame front, and there is still a distance between the leading shock wave and the flame front. For a tube with multiple fluidic obstacles, the local explosion is triggered not only in the boundary layer but also on the flame front, where the flame caught up with the leading shock wave. The DDT distance and time of the case with multiple fluidic obstacles are shorter compared with the multiple solid obstacles case, about a decrease of 36% and 40%, respectively.

Transverse jet composition

Because of the potential risk of backfire in actual experiments that use premixed gas as fluidic obstacle, oxygen and diluted gas are generally employed as fluidic obstacle in the experiments. However, the fluidic obstacle composed of oxygen and diluted gases has a considerable influence on the local mixing and homogeneity of the mixture, and hence

affects the flame acceleration and DDT. The velocity curve of flame propagation in the tube with a single fluidic obstacle (T_{jet} = 300K, PR = 3) composed of different components can be seen in Fig. 8. The result shows that using a premixed reactive fluidic obstacle enhances flame acceleration, while the cases with obstacles of argon and oxygen need more time to transition to detonation. The dotted line shows the theoretical CJ detonation velocity at the initial condition, which is about 1783m/s, as calculated by Cantera. The detonation wave speed gradually decreases to the CJ velocity after the overdriven state. Note that using premixed reactive gas as the fluidic obstacle leads to a higher overdriven detonation velocity of about 2772 m/s, and shortens the DDT distance by 41.6% and the DDT time by 42.2% compared with the smooth tube condition.

In order to investigate the effect of fluidic injection on local reactive concentration of the flow field, the local oxygen mass fraction Y_O_2 and equivalence ratio (ER) are calculated considering the ratio of hydrogen to oxygen as shown in Figure 9. The ER is unchanged after injection of premixed gas with the same composition of the mainstream (Figure 9 a, d). The oxygenous obstacle has a greater impact on the local ER. There are some regions containing pure oxygen especially near the injection nozzle exit. The mixing between fluidic obstacle and mainstream is incomplete, as a result, a lean unburned zone is formed downstream (Figure 9 b, e). When the obstacle is composed of pure argon, the ER only changes in the region near the injection nozzle, and other regions are still stoichiometric (Figure 9 c, f). However, the local oxygen concentration declines due to the inert gas, which is not conducive to the flame acceleration.

Table 1 presents the values of DDT distance and time within various conditions. Compared with the smooth tube condition, the DDT distance of the case with inert fluidic obstacle can be shortened by 22.5%, and the DDT time can be shortened by 20.8%. Further, the DDT distance with argon obstacle (254.51 mm) is shorter than that of the

single solid obstacle case (287.47 mm, BR = 0.5), while the DDT time of the argon obstacle case (0.937 ms) is greater than that of the single solid obstacle case (0.983 ms, BR = 0.5). This means that the flame influenced by the inert obstacle undergoes a relatively long acceleration period but with a higher accelerated rate in comparison with the solid obstacle case. Because the fluidic obstacle with premixed reactive gas has a positive effect on shortening DDT distance and time, in the following three sections, a mixture with the same concentration as the gas in the tube is used as transverse jet.

Transverse jet temperature

Figure 10 shows the DDT distance and DDT time of flames at different initial stagnation temperatures for the fluidic obstacle (PR = 5). With the increase of the initial fluidic temperature, the distance and time required for the transition decrease first and then increase within a narrow range. The fluidic obstacle is influenced by the mainstream unburned gas, and a series of vortices moves downstream. When its initial stagnation temperature rises, the energy per unit time injected into the flow field increases. Increasing temperature can solve the problem of local static temperature drop caused by a high-speed fluidic obstacle, and the movement of fluid vortices downstream can preheat the unburned gas, which is conducive to flame propagation. However, if the initial stagnation temperature of the fluidic obstacle is too high, i.e. above its auto-ignition temperature, the jet injected into the flow field is no longer completely unburned premixed gas, but the mixture of premixed gas and combustion products. Under this condition, the fluidic obstacle is closer to a hot jet used in the detonation engine to initiate detonation directly. Some complex critical parameter values of a hot jet influencing the effect on unburned mixture has been investigated in previous studies (Carnasciali et al., 1991; Dorofeev et al., 1996; Han et al., 2013; Cai et al., 2014). This is another field reserved for further discussion. ~~On the one hand, the high temperature gas can preheat~~

~~the unburned mainstream premixed gas, which advances the transition; on the other hand, the jet composed of combustion products can dilute the local premixed gas, resulting in a decrease of the local heat release rate.~~

In addition, it is noted that the increasing temperature of the fluidic obstacle will decrease the velocity and mass flow rate. The high-temperature gas can preheat the unburned premixed mainstream, but the decreasing flow rate constrains this positive effect. Besides, decreasing the velocity of the fluidic obstacle weakens its penetrating power and thereby induces fewer vortices. As shown in Fig. 11, the flame surface with a high-temperature fluidic obstacle is less folded when the flame interacts with the vortices, because the high-temperature vortices are more easily ignited. Such factors have a negative influence on flame propagation because the wrinkling and expansion of the flame front are the main reasons for flame acceleration at the initial stage. When the initial stagnation temperature of the fluidic obstacle rises to 800K, on the contrary, the DDT distance and time rise before a slight fall at 900K. However, the increased temperature of the fluidic obstacle has a limited effect on DDT time and distance, because the amount of injected gas is small compared to the whole unburned gas.

Transverse jet pressure

Figure 12 reveals the DDT distance and time for various initial jet stagnation pressures in the detonation duct. In this section, the stagnation temperature of all the transverse jet is 700K. With the increase of jet initial pressure, the run-up to detonation distance and time are decreasing. When the jet's initial stagnation pressure rises from 0.3 MPa to 0.5 MPa, the DDT distance and time are reduced by 38.0% and 23.3% on average. But the positive effect of increasing the jet pressure is weakened when the initial jet pressure continues to rise. When the jet initial pressure is 0.9 MPa and the stagnation temperature is 700 K, the DDT distance (69.7 mm) is the shortest.

On the one hand, the increasing initial jet pressure raises the jet flow rate and the jet momentum, which adds extra energy to the unburned mixture in the local flow field and enhances the energy release when the flame propagates there; on the other hand, the high-pressure jet produces compression waves, which move upstream and interact with the initial flame surface. The flame surface is more likely unstable because of those compression waves and it has a positive effect on the flame initial acceleration process.

As shown in Fig. 13, within the same jet stagnation temperature (700K), the pressure data are sampled every 0.1 ms along the central axis of the direction of flame propagation from 0 to 0.8 ms. The dashed lines in the picture indicate the theoretical CJ pressure. In this figure, with the increase of the jet initial pressure, the flame and the detonation wave propagate further at the same time. The pressure peak gradually decreases and tends to be stable, which corresponds to the detonation wave speed gradually decreasing and finally being near CJ velocity. The overdriven detonation decays to a stable detonation. In addition, compression waves are observed in the flow field and strengthened over time.

At the initial stage, a pressure reduction is observed around the jet injection region, which is due to the vortices induced by the jet flow at the sampling point and the center of them is usually of low pressure (shown in Figure 14 a.). When the flame approaches the jet, the vortices are moving downstream (shown in Figure 14 b.) because of the unburned mainstream flow and the pressure of the position near the jet exit is increasing. The leading compression wave is increasingly strengthened (shown in Figure 14 c.). As the transition to detonation is completed (shown in Figure 14 d.), the pressure around the jet location is much higher than before. For some cases, like initial pressure being 0.3 MPa or 0.5 MPa, the pressure in the tube is even greater than the injection pressure, which means that the jet flow cannot be successfully injected into the flow field

anymore. It is beneficial to utilize a higher initial pressure jet as fluidic obstacles in the detonation engine; but it remains an engineering challenge to provide an extra higher-pressure reactive jet.

The fluidic obstacle induces vortices and enhances the perturbation in the main flow; on the other hand, the relatively high-pressure jet also increases the local static pressure of the unburned mixture in the tube and the flame should also be accelerated. An idealized situation is therefore calculated to measure the effect of static pressure increases on the DDT process. As Fig. 15 shows, a fluidic obstacle will increase the pressure in a local region, which is estimated by the volume from the left wall to the location of DDT. The jet duration is equal to the DDT time. It should be noted that the mass flow rate of a fluidic obstacle is changing with the pressure of the main flow. Therefore, in this ideal model the mass flow rate maximum is taken as the calculated average value to estimate the pressure rise in the tube. Then the increased pressure P_{incr} is set as the initial pressure P_{init} in a smooth tube as contrast condition, c.f. Table 2.

Figure 16 shows the decrease of DDT distance and time when the fluidic obstacle is added compared to increasing the initial pressure of a smooth tube. When the initial pressure of the fluidic obstacle is 0.3MPa or 0.5MPa, the cases with fluidic obstacle can shorten the DDT distance and time more than the smooth tube even when the pressure is higher than the real pressure increased by the fluidic obstacle. However, the influence of pressure increases in the tube plays a more important role as the jet initial pressure rises. The equivalent models, a smooth tube with high initial pressure, can shorten DDT distance and time more than the cases with fluidic obstacle. In other words, the effects of flow disturbance and vortices in the tube are no longer the main reason for DDT distance and time decrease when the pressure of the fluidic obstacle is relatively high.

Transverse jet nozzle width

The jet width, namely the jet mass flow rate, is also an important parameter in fluidic obstacle design. Figure 17 indicates the density gradient magnitude change of the local flow field in cases of different jet widths at the same time (0.12ms). The jet enters from the bottom wall and forms the rotating coherent structures, denoted as “mushroom vortices” (Huang and Lan, 2005). The mushroom structure is composed of a pair of counter-rotating vortices, of which the right side rotates clockwise, while the left side rotates counterclockwise. The follow-up trailing vortex caused by Kelvin-Helmholtz instability rises vertically and joins into the leading mushroom vortices.

Because the back pressure of the jet exit is influenced by the mainstream, it is difficult to define the accurate jet mass flow rate. However, the mass flow rate is linearly proportional to the width of the exit when the jet initial pressure, temperature and components are the same. In those cases, the increase on jet flow rate not only changes the structure of mushroom vortices, like increasing the area and curvature of vortices surface, but also induces enhanced compression waves. As shown in Fig. 17, extra compression waves are observed in the wider jet cases. The first pressure wave expands to the flow field spherically and collides with the upper wall; then, the reflected pressure wave moves towards the flame front as indicated by dotted arrows in this figure. The interaction between the pressure wave and flame front promotes the flame instability and acceleration.

Fig. 18 shows the effects of jet width on DDT distance and time for the same temperature and pressure. When the jet width increases from 1 mm to 8 mm, the DDT distance drops from 213.87 mm to 127.28 mm and the DDT time drops from 0.90 ms to 0.53 ms, respectively. The jet width has a distinct effect on the flame propagation and DDT process compared with cases changing jet initial pressure or temperature, in which

all the widths is set as 2 mm. There might be some differences when the jet width is larger, like 4 mm or 8 mm, which needs further calculation cases in the future.

Conclusions

In the present study, two-dimensional numerical simulations based on the open-source program AMROC have been conducted to investigate the effects of transverse jets on flame acceleration and DDT under different jet initial conditions.

Injecting transverse jets in the tube can accelerate the flame propagation and advance the transition to detonation. The effect of using a premixed gas jet with the same concentration as the mainstream as the fluidic obstacle to accelerate the flame is better than that of a solid obstacle. Different mixture compositions of the fluidic obstacle also have an influence on the equivalence ratio of the local flow field. The acceleration effect of a single premixed gas obstacle with the same concentration is better than that of a single diluted gas obstacle. However, compared with the smooth tube condition, the argon obstacle can still shorten the DDT distance by 22.5% and the DDT time by 20.8%.

The distance and time of DDT decrease first and then increase with the increase of the initial stagnation temperature of the fluidic obstacle. Increasing the initial temperature of the obstacle can heat the unburned gas, which is conducive to flame propagation. On the other hand, with the increase of initial stagnation temperature of the fluidic obstacle, the mass flow rate and momentum of the jet will decline. As a result, the penetrating power of the fluidic obstacle is weakened and the flame is less folded, which is not beneficial to flame acceleration. The DDT distance and time shorten with the increases of the initial stagnation pressure of the fluidic obstacle which increases the static pressure and the kinetic energy of the unburned gas in the flow field. Moreover, the high-pressure or wide jet injected into the mainstream can produce compression waves. These waves interact with the flame surface at the initial propagating stage and lead to

unsteadiness of the flame surface, which can benefit the flame acceleration at the initial stage.

Funding

This work was supported by the National Natural Science Foundation of China under Grant [number 51876182 and 51406171]; Fundamental Research Funds for the Central Universities of China under Grant [number 20720180058]; Aeronautics Power Foundation under Grant [number 6141B090325].

References

Eichert, H., and Fischer, M. 1986. Combustion-related safety aspects of hydrogen in energy applications. *Int. J. Hydrogen Energy*, **11**,11. doi:10.1016/0360-3199(86)90049-2

Roy, G.D., Frolov, S.M., Borisova, A.A., and Netzer, D.W. 2004. Pulse detonation propulsion: challenges, current status, and future perspective. *Prog. Energy Combust. Sci*., **30**, 545. doi: 10.1016/j.pecs.2004.05.001

Petukhov, V.A., Naboko, I.M., and Fortov, V.E. 2009. Explosion hazard of hydrogen-air mixtures in the large volumes. *Int. J. Hydrogen Energy*, **34**, 24. doi: 10.1016/j.ijhydene.2009.02.064

Lee, J.H.S. 2008. The Detonation Phenomenon. Cambridge University Press, London.

Lee, S.Y., Watts, J., Saretto, S., Pal, S., Conrad, C., Woodward, R., and Santoro, R. 2004. Deflagration to detonation transition processes by turbulence-generating obstacles in pulse detonation engines. *J. Propul. Power*, **20**, 1026. doi: 10.2514/1.11042

Ciccarelli, G., and Dorofeev, S. 2008. Flame acceleration and transition to detonation in ducts. *Prog. Energy Combust. Sci.*, **34**, 499. doi: 10.1016/j.pecs.2007.11.002

Oran, E.S., and Gamezo, V.N. 2007. Origins of the deflagration-to-detonation transition in gas-phase combustion. *Combust. Flame*, **148**, 4. doi: 10.1016/j.combustflame.2006.07.010

Gamezo, V.N., Ogawa, T., and Oran, E.S. 2007. Numerical simulations of flame propagation and DDT in obstructed channels filled with hydrogen-air mixture. *Proc. Combust. Inst.*, **31**, 2463. doi: 10.1016/j.proci.2006.07.220

Ayu, A., Nobuyuki, T., Edyta, D., and Koichi, H. A. 2018. Two-dimensional numerical simulation of detonation transition with multi-step reaction model: effects of obstacle height. *Combust. Sci. Technol.*, **191**, 4. doi:10.1080/00102202.2018.1498849

Kessler, D.A., Gamezo, V.N., and Oran, E.S. 2010. Simulations of flame acceleration and deflagration-to-detonation transitions in methane-air systems. *Combust. Flame*, **157**, 2063. doi: 10.1016/j.combustflame.2010.04.011

Gamezo, V.N., Ogawa, T., and Oran, E.S. 2008. Flame acceleration and DDT in channels with obstacles: Effect of obstacle spacing. *Combust. Flame*, **155**, 302. doi: 10.1016/j.combustflame.2008.06.004

Johansen, C., and Ciccarelli, G. 2010. Numerical simulations of the flow field ahead of an accelerating flame in an obstructed channel. *Combust. Theor. Model*, **14**, 235. doi: 10.1080/13647830.2010.483020

Knox, B.W. 2011. The Fluidic Obstacle Technique: An Approach for Enhancing Deflagration to-Detonation Transition in Pulsed Detonation Engines. M.S. Thesis, The State University of New York at Buffalo.

Yuan, L. L., and Street, R. L. 1998. Trajectory and entrainment of a round jet in crossflow. *Phys. Fluids*, **10**, 2323. doi: 10.1063/1.869751

Karagozian, and Ann, R. 2014. The jet in crossflow. *Phys. Fluids*, **26**, 101303. doi: 10.1063/1.4895900

Knox, B.W., Forliti, D.J., Stevens, C.A., Hoke, J.L., and Schauer, F.R. 2010. Unsteady flame speed control and deflagration-to-detonation transition enhancement using fluidic obstacles. In *Proceedings of the 48th AIAA Aerospace Sciences Meeting and Exhibit Conference*, Orlando, Paper No. 2010-151.doi: 10.2514/6.2010-151

Knox, B.W., Forliti, D.J., Stevens, C.A., Hoke, J.L., and Schauer, F.R. 2011. A comparison of fluidic and physical obstacles for deflagration-to-detonation transition. In *Proceedings of the 49th Aerospace Sciences Meeting and Exhibit Conference*, Orlando, Paper No. 2011-587.doi: 10.2514/6.2011-587

Zhao, S., Fan, Y., Lv, H., and Jia, B. 2017. Effects of a jet turbulator upon flame acceleration in a detonation tube. *Appl. Therm. Eng.*, **115**, 33. doi: 10.1016/j.applthermaleng.2016.12.068

McGarry, J.P., and Ahmed, K.A. 2015. Laminar deflagrated flame interaction with a fluidic jet flow for deflagration-to-detonation flame acceleration. In *Proceedings*

of the 51st AIAA/SAE/ASEE Joint Propulsion Conference, Orlando, Paper No. 2015-4096. doi: 10.2514/6.2015-4096

Chambers, J., and Ahmed, K.A. 2017. Turbulent flame augmentation using a fluidic jet for Deflagration-to-Detonation. *Fuel*, **199**, 616. doi: 10.1016/j.fuel.2017.03.023

McGarry, J.P., and Ahmed, K.A. 2017. Flame-turbulence interaction of laminar premixed deflagrated flames. *Combust. Flame*, **176**, 439. doi: 10.1016/j.combustflame.2016.11.002

Wang, Y.J., Fan, W., Li, S.X., Zhang, Q.B., and Li, H.B. 2017. Numerical simulations of flame propagation and DDT in obstructed detonation tubes filled with fluidic obstacles. In *Proceedings of the 21st AIAA International Space Planes and Hypersonic Technologies Conference*, Xiamen, Paper No. 2017-2382. doi: 10.2514/6.2017-2382

Peng, H., Huang, Y., Deiterding, R., Luan, Z.Y., Xing, F., and You, Y.C. 2018. Effects of jet in crossflow on flame acceleration and deflagration to detonation transition in methane–oxygen mixture. *Combust. Flame*, **198**, 69. doi: 10.1016/j.combustflame.2018.08.023

Zeldovich, Y.B. 1980. Regime classification of an exothermic reaction with nonuniform initial conditions. *Combust. Flame*,**39**, 211. doi: 10.1016/0010-2180(80)90017-6

Liberman, M.A., Ivanov, M.F., Kiverin, A.D., Kuznetsov, M.S., Chukalovsky, A.A., and Rakhimova, T.V. 2010. Deflagration-to-detonation transition in highly reactive combustible mixtures. *Acta Astronautica*, **67**, 688. doi: 10.1016/j.actaastro.2010.05.024

Zhang, Y.L., Zhou, L., Gong, J.S., Ng, H.D., and Teng, H.H. 2018. Effects of activation energy on the instability of oblique detonation surfaces with a one-step chemistry model. *Phys. Fluids*, **30**, 106110. doi: 10.1063/1.5054063

Lee, J.H.S., and Moen, I.O. 1980. The mechanism of transition from deflagration to detonation in vapor cloud explosion, *Prog. Energy Combust.*,**6**, 359. doi: 10.1016/0360-1285(80)90011-8

Edyta, D., and Hayashi, A.K.2013. Auto-ignition and DDT driven by shock wave – Boundary layer interaction in oxyhydrogen mixture. *Int. J. Hydrogen Energy*, **38**, 4185. doi: 10.1016/j.ijhydene.2013.01.111

Deiterding, R. 2003. Parallel adaptive simulation of multi-dimensional detonation structures. Ph.D. thesis, Brandenburg University of Technology Cottbus–Senftenberg.

Deiterding, R. 2009. A parallel adaptive method for simulating shock-induced combustion with detailed chemical kinetics in complex domains. *Comput. Struct.*,**87**, 769. doi: 10.1016/j.compstruc.2008.11.007

Ziegler, J.L., Deiterding, R., Shepherd, J.E., and Pullin, D.I. 2011. An adaptive high-order hybrid scheme for compressive, viscous flows with detailed chemistry. *J. Comput. Phys.*, **230**, 7598.doi: 10.1016/j.jcp.2011.06.016

Deiterding, R., and Wood, S. 2013. Parallel adaptive fluid-structure interaction simulation of explosions impacting on building structures. *Comput. Fluids*,**88**, 719.doi: 10.1016/j.compfluid.2013.05.009

Cai, X.D., Liang, J.H., Deiterding, R., Mahmoudi, Y., and Sun, M.B. 2018. Experimental and numerical investigations on propagating modes of detonations: Detonation wave/boundary layer interaction. *Combust. Flame*, **190**, 201. doi: 10.1016/j.combustflame.2017.11.015

Cai, X.D., Liang, J.H., Deiterding, R., Che, Y.G., and Lin, Z.Y. 2016. Adaptive mesh refinement based simulations of three-dimensional detonation combustion in supersonic combustible mixtures with a detailed reaction model. *Int. J. Hydrogen Energy*, **41**, 3222. doi: 10.1016/j.ijhydene.2015.11.093

Wang, Y., Han, W., Deiterding, R., and Chen, Z. 2018. Effects of disturbance on detonation initiation in $H_2/O_2/N_2$ mixture. *Phys. Rev. Fluids*, **3**, 123201. doi: 10.1103/PhysRevFluids.3.123201

Westbrook, C.K. 1982. Chemical kinetics of hydrocarbon oxidation in gaseous detonations. *Combust. Flame*, **46**, 191.doi: 10.1016/0010-2180(82)90015-3

Goodwin D. G., Speth R. L., Moffat H. K., and Weber B. W. 2018 Cantera: An object-oriented software toolkit for chemical kinetics, thermodynamics, and transport processes. https://www.cantera.org, 2018. Version 2.4.0. doi:10.5281/zenodo.1174508

Han, W.H., Gao, Y., and Law, C.K. 2017. Flame acceleration and deflagration-to-detonation transition in micro- and macro-channels: An integrated mechanistic study. *Combust. Flame*, **176**, 285. doi: 10.1016/j.combustflame.2016.10.010

Carnasciali, F., Lee, J.H.S., Knystautas, R., and Fineschi, F.1991. Turbulent jet initiation of detonation. *Combust. Flame*, **84**, 170. doi: 10.1016/0010-2180(91)90046-E

Dorofeev, S.B., Bezmelnitsin, A.V., Sidorov, V.P., Yankin, J.G., and Matsukov, I.D. 1996. Turbulent jet initiation of detonation in hydrogen-air mixtures. *Shock Waves*, **6**, 73. doi: 10.1007/BF02515190

Han, X., Zhou, J., Lin, Z.Y., and Liu, Y. 2013. Deflagration-to-detonation transition induced by hot jets in a supersonic premixed airstream. *Chin. Phys. Lett.*, **30**, 054701. doi: 10.1088/0256-307X/30/5/054701

Cai, X.D., Liang, J.H., Lin, Z.Y., Deiterding, R., and Liu, Y. 2014. Parametric study of detonation initiation using a hot jet in supersonic combustible mixtures. *Aerosp. Sci. Technol.* ,**39**, 442. doi: 10.1016/j.ast.2014.05.008

Huang, R.F., and Lan, J. 2005. Characteristic modes and evolution processes of shear-layer vortices in an elevated transverse jet. *Phys. Fluids*, **17**, 034103. doi: 10.1063/1.1852575

Table 1. DDT distance and time of different cases

Case		DDT distance (mm)	DDT time (ms)
Smooth tube		333.17	1.242
Solid obstacle (BR = 0.1)		314.88	1.137
Solid obstacle (BR = 0.5)		287.47	0.937
Fluidic obstacle (T_{jet} = 300K, PR = 3)	Mixture	194.60	0.718
	Oxygen	219.08	0.818
	Argon	254.51	0.983

Table 2. Estimated pressure increases influenced by the fluidic obstacle.

Fluidic obstacle		P_{init} in smooth tube
Temperature and pressure	P_{incr}	
300K & 0.3MPa	0.1179MPa	0.1179MPa
300K & 0.5MPa	0.1617MPa	0.1617MPa
300K & 0.7MPa	0.1868MPa	0.1868MPa
300K & 0.9MPa	0.2201MPa	0.2201MPa

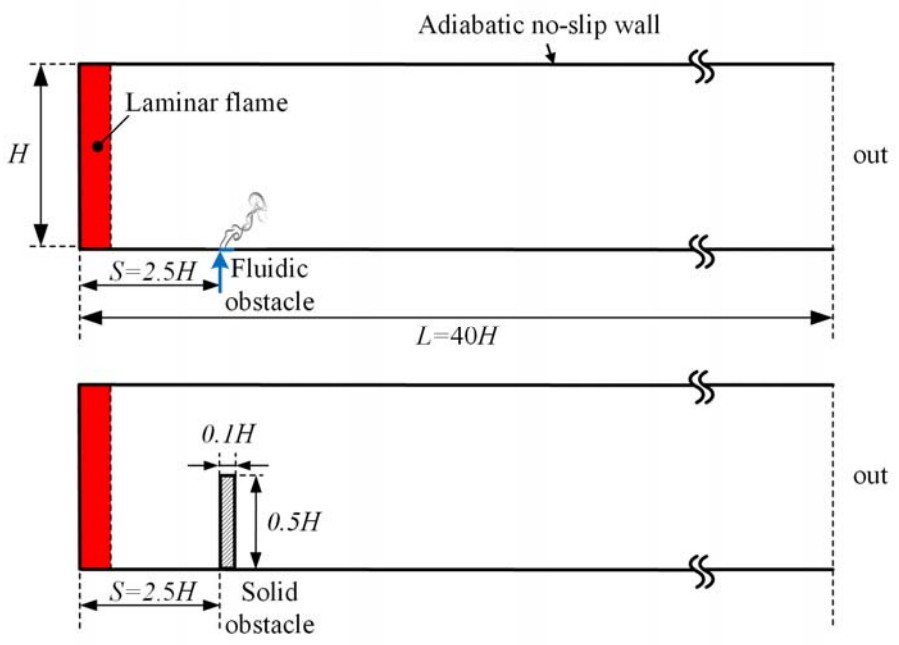

Figure 1. Schematic diagram of the computational domain

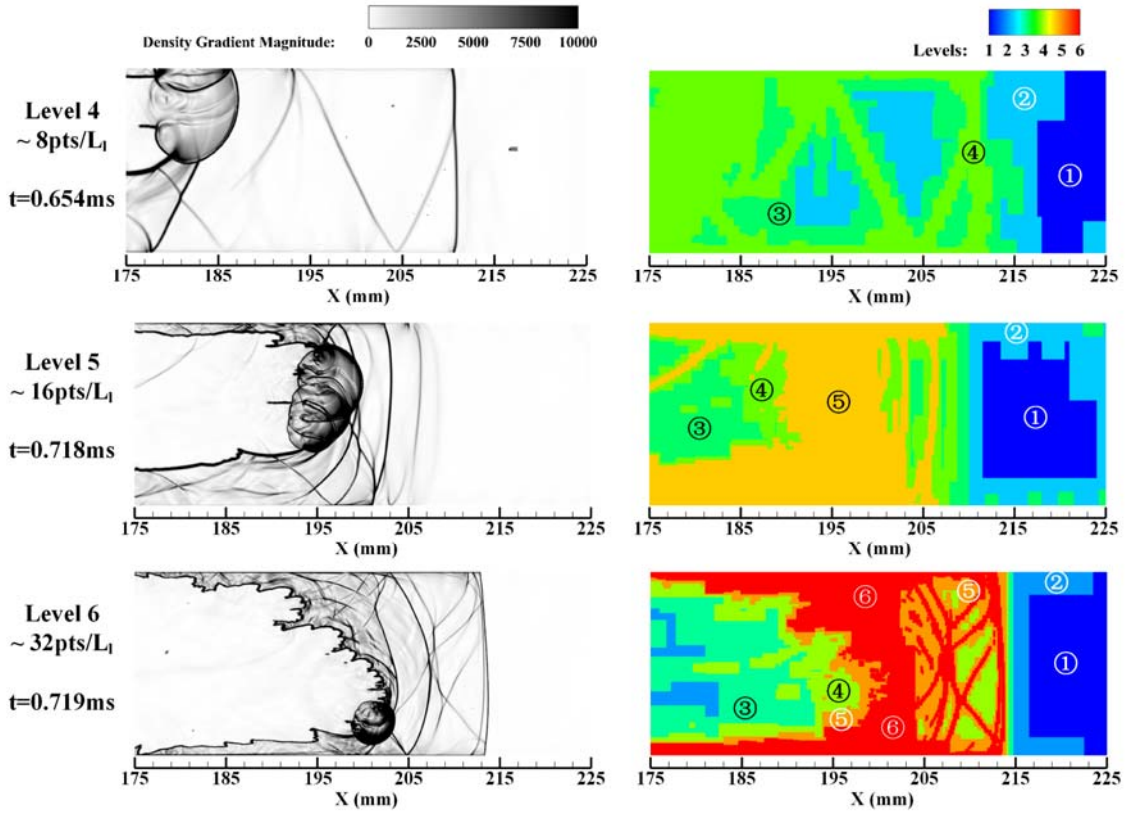

Figure 2. Diagram of density gradient magnitude (left) and distribution of different mesh refinement levels, indicated by color (right)

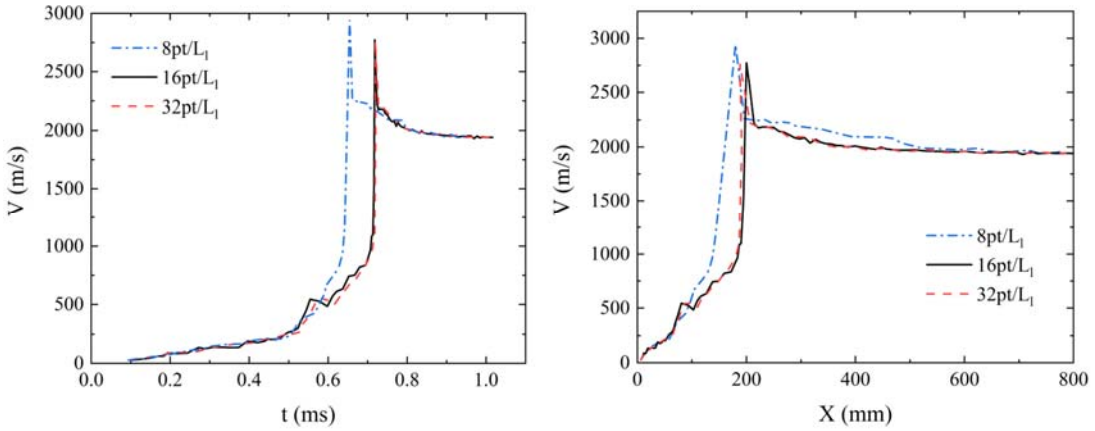

Figure 3. Diagram of flame front propagation velocity for different spatial resolutions

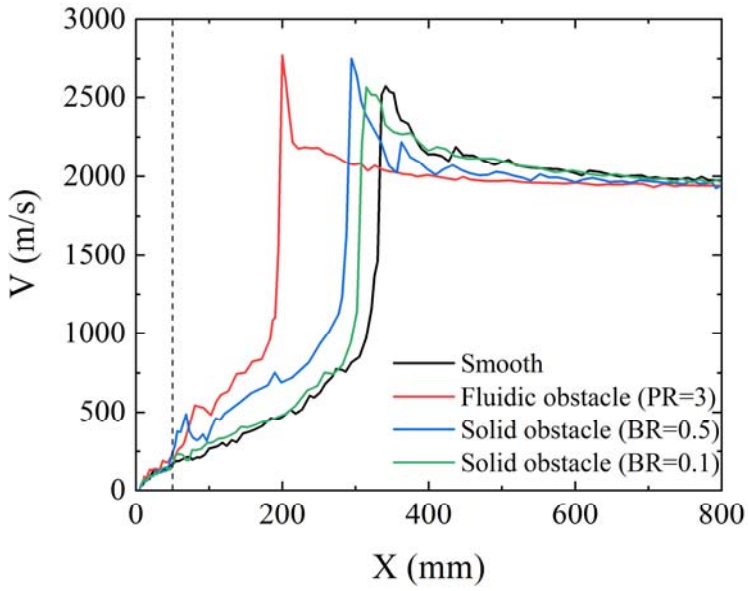

Figure 4. Diagram of flame front propagation velocity versus distance between smooth tube and tubes with a single obstacle.

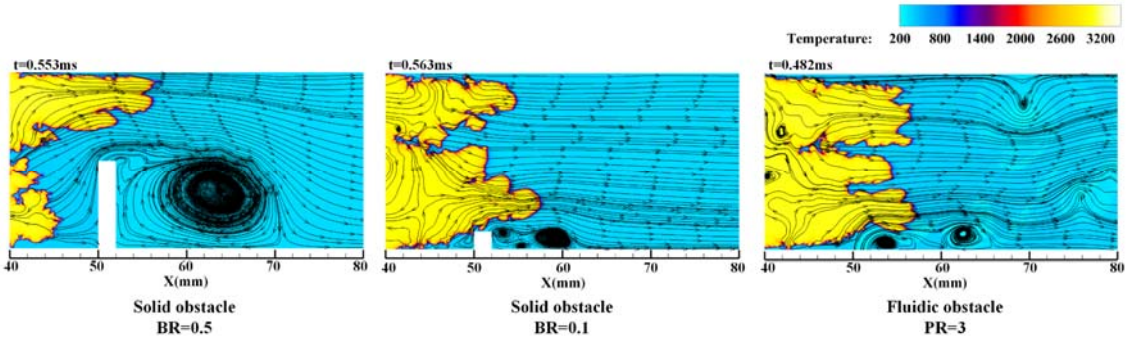

Figure 5. Temperature and streamline profile when the flame front interacts with the obstacle.

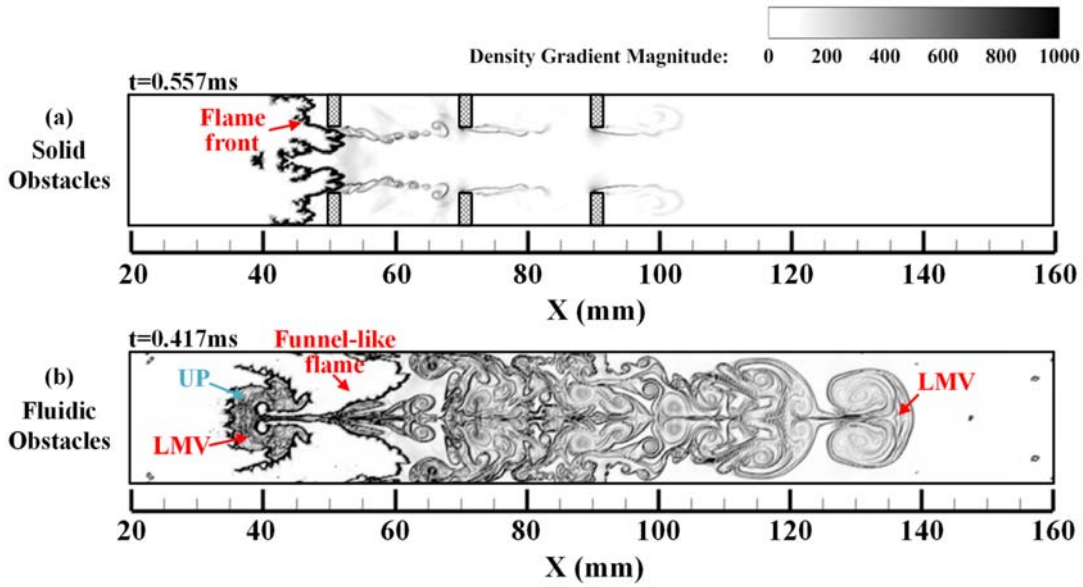

Figure 6. Diagram of the interaction of flame and multiple obstacles (LMV: leading mushroom vortices; UP: unburned pocket).

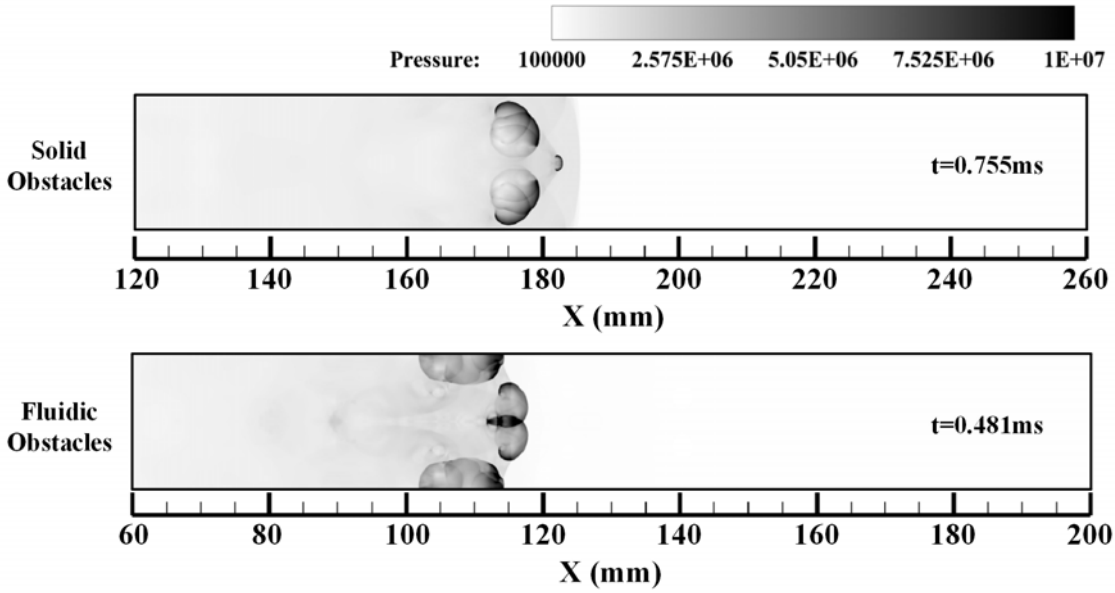

Figure 7. Pressure contours of cases with multiple obstacles at the time at which the local explosion is occurring.

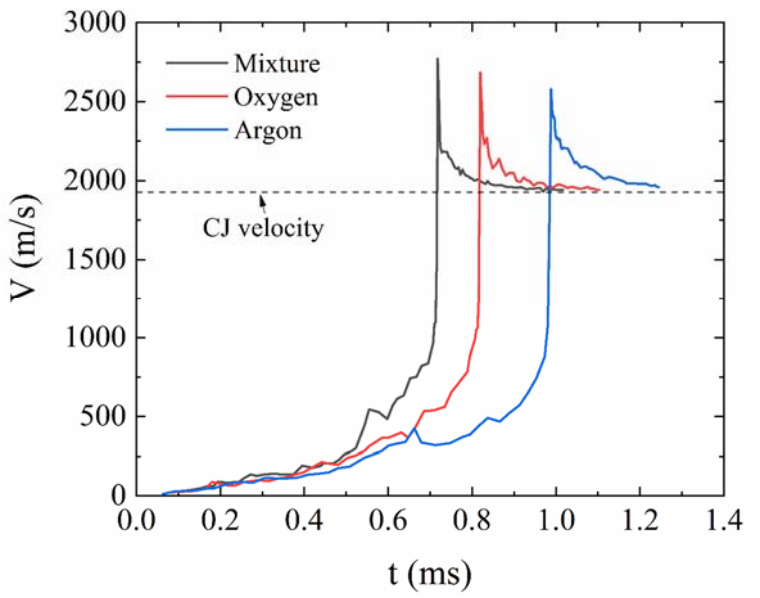

Figure 8. Diagram of flame front propagation velocity versus time between tubes with different fluidic obstacle composition.

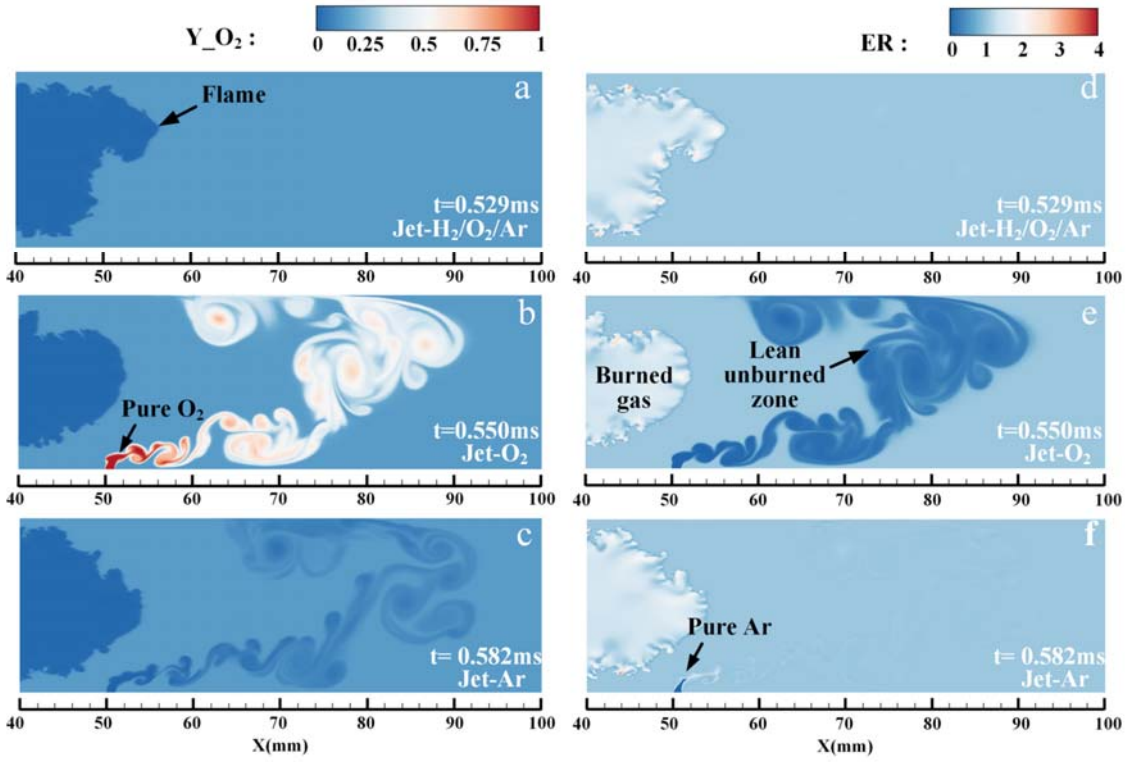

Figure 9. Locally enlarged segments of equivalence ratio and density profile.

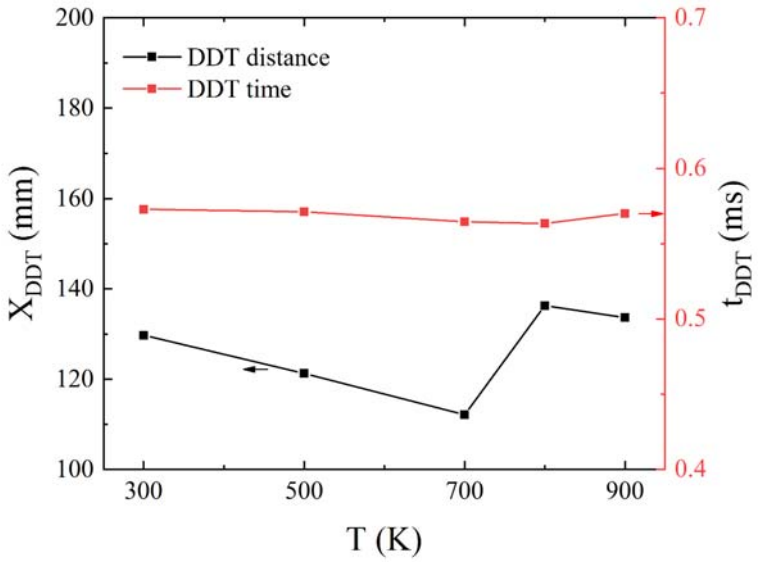

Figure 10. DDT distance and time for different initial temperatures of the fluidic obstacle.

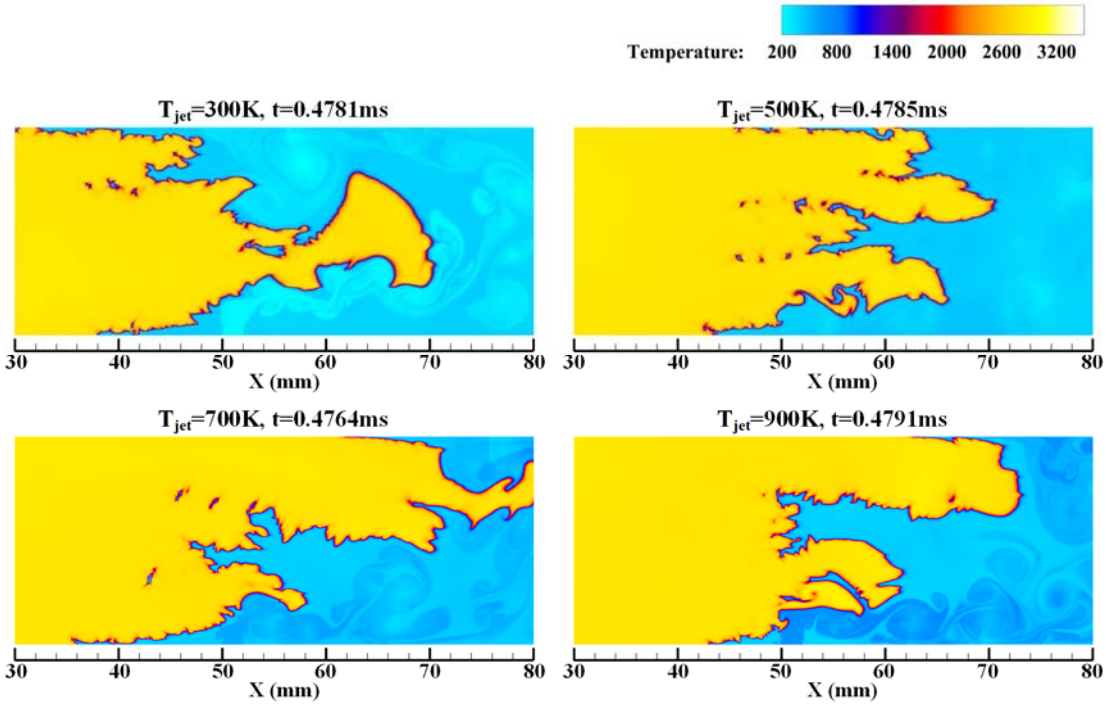

Figure 11. Temperature contours of various cases at the time at which the flame front is interacting with a single fluidic obstacle (T_{jet} is the stagnation temperature of the fluidic obstacle).

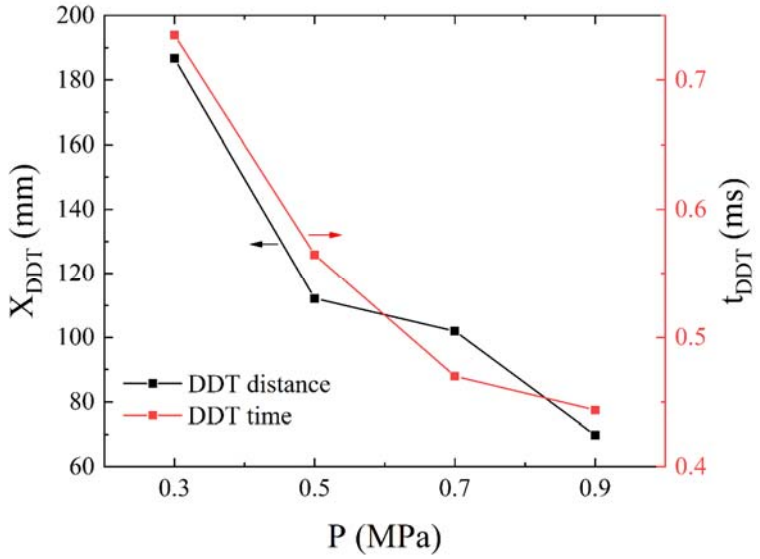

Figure 12. The DDT distance and time for different initial stagnation pressures of the fluidic obstacle.

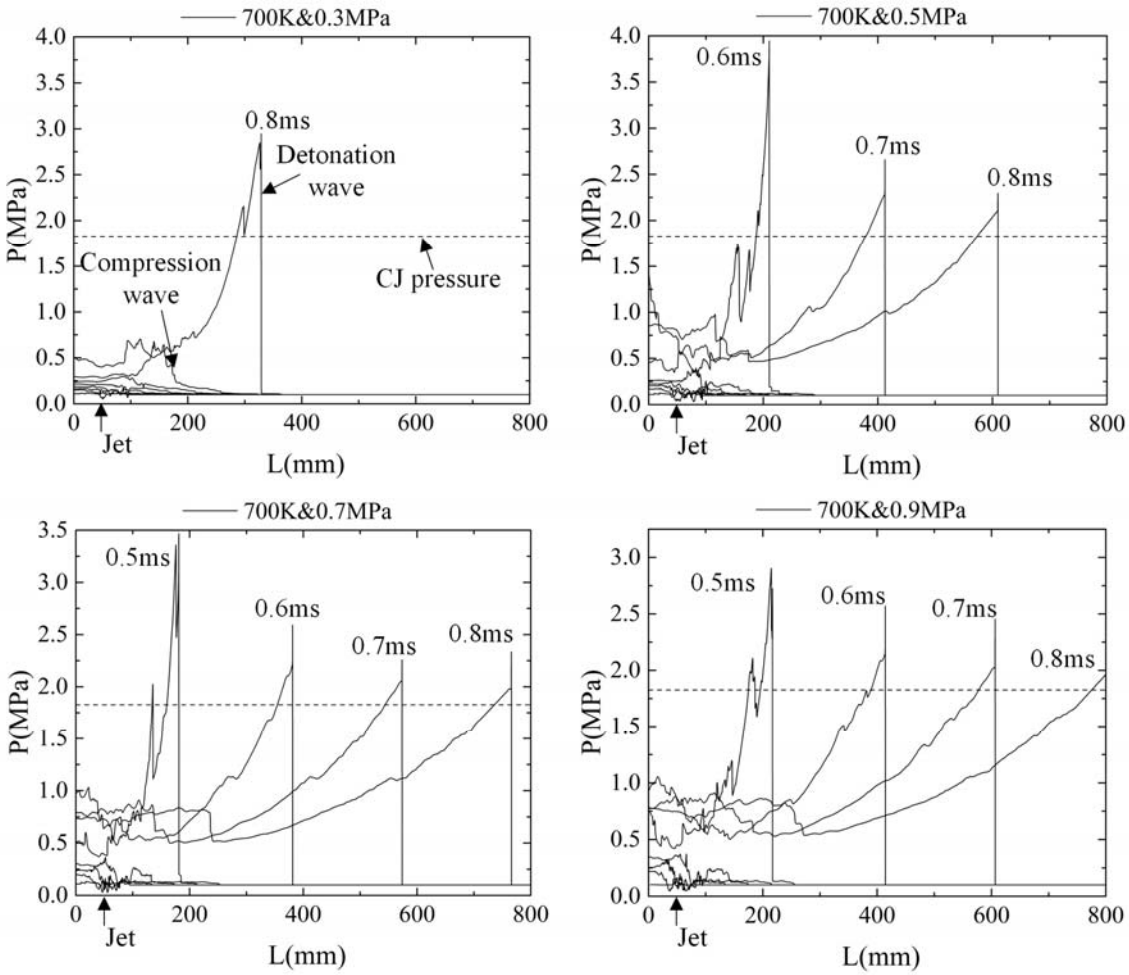

Figure 13. Pressure records along the center line tube for eight time instances (0~0.8ms, △=0.1ms).

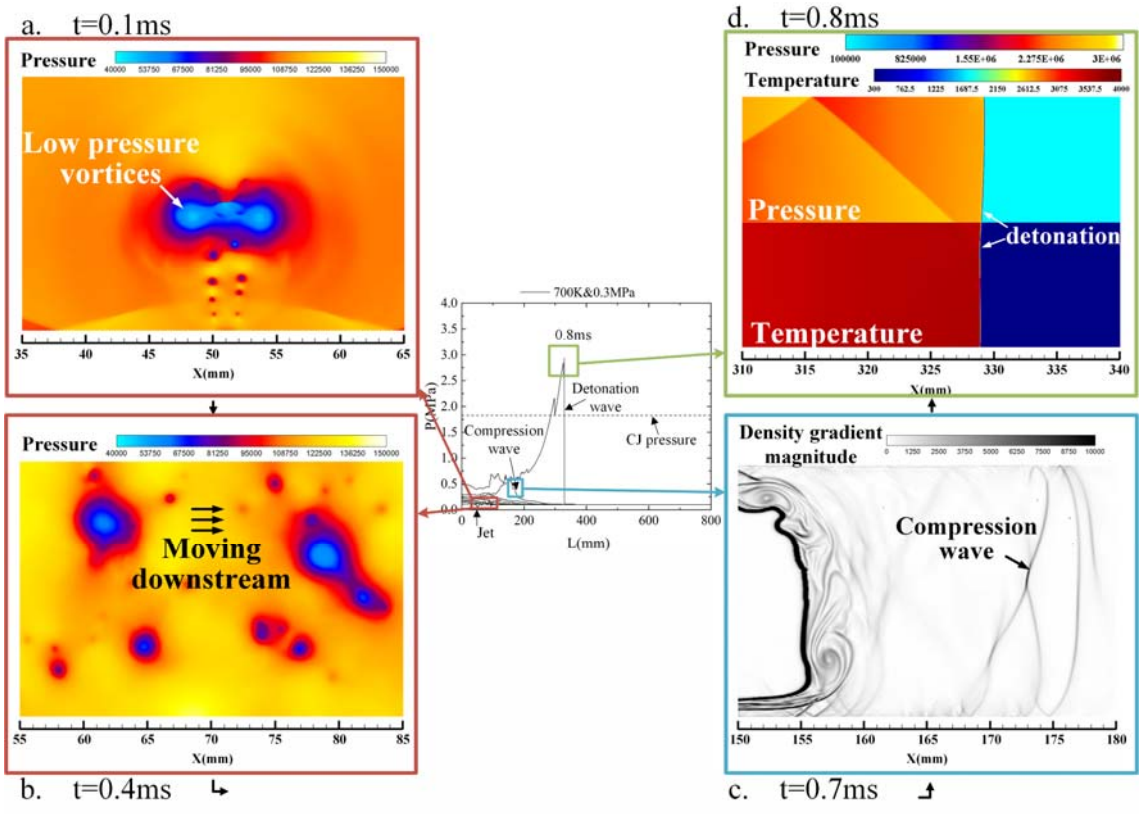

Figure 14. Sequence diagram of local enlarged flow field with pressure changes

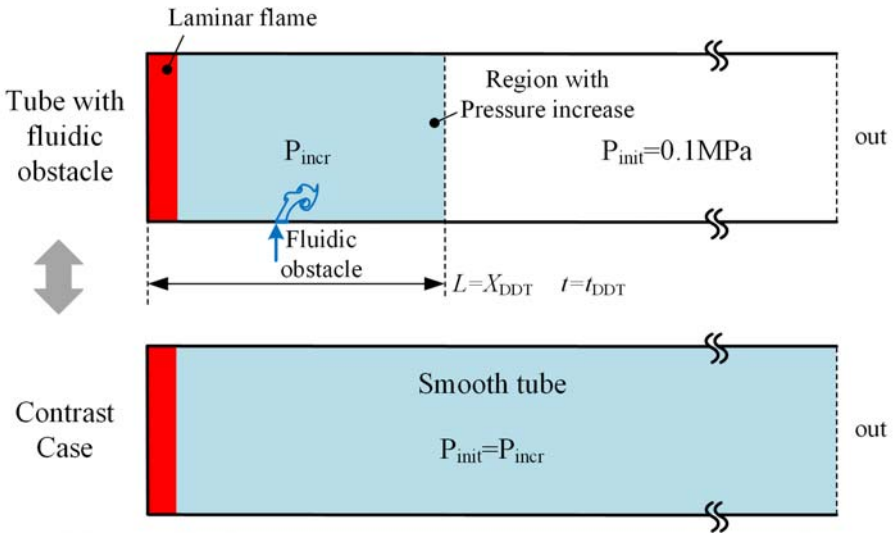

Figure 15. Schematic diagram of the simplified equivalent models about local pressure increase.

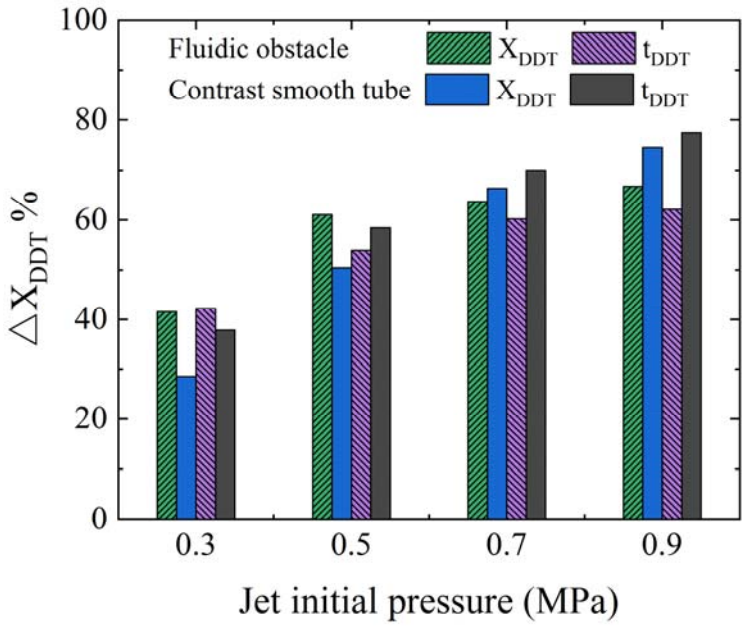

Figure 16. The decrease in DDT distance and DDT time of a tube with fluidic obstacle or higher initial pressure (Compared case: smooth tube, initial pressure equals to 0.1MPa).

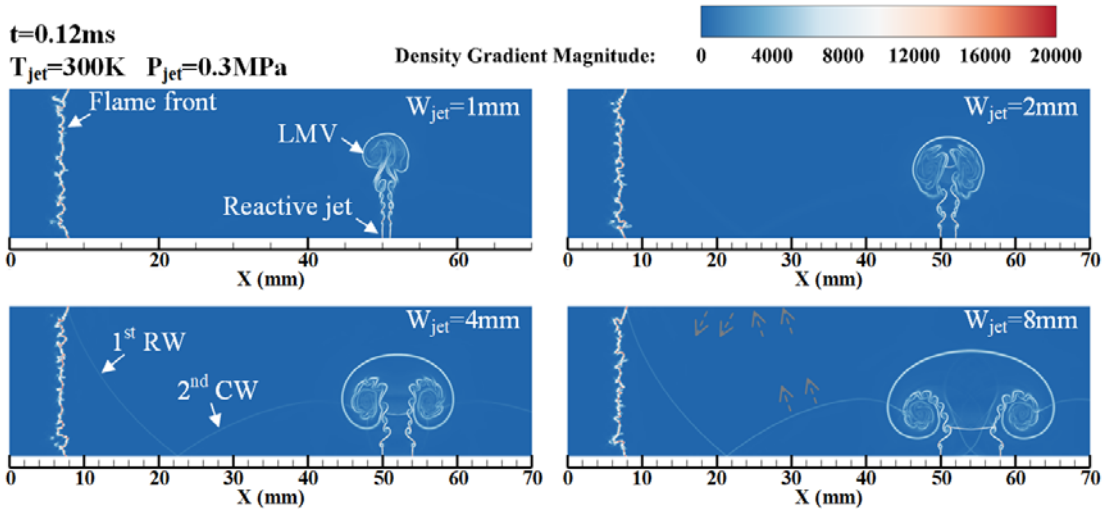

Figure 17. Diagram of density gradient magnitude in local flow field at 0.12ms (LMV: leading mushroom vortices; RM: reflected pressure wave; CW: compression wave).

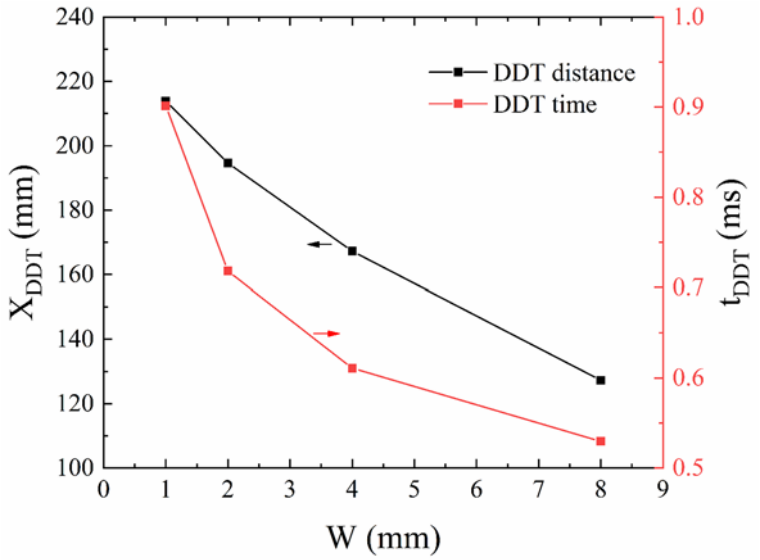

Figure 18. The DDT distance and time for different fluidic obstacles jet widths.